# Evolution of the electronic and ionic structure of Mg clusters with increase in cluster size

Andrey Lyalin,* Ilia A. Solov'yov,† Andrey V. Solov'yov,‡ and Walter Greiner
*Institut für Theoretische Physik der Universität Frankfurt am Main, Robert-Mayer Strasse 8-10, D-60054 Frankfurt am Main, Germany*
(Received 27 November 2002; revised manuscript received 5 February 2003; published 24 June 2003)

The optimized structure and electronic properties of neutral and singly charged magnesium clusters have been investigated using *ab initio* theoretical methods based on density-functional theory and systematic post–Hartree-Fock many-body perturbation theory accounting for *all* electrons in the system. We have systematically calculated the optimized geometries of neutral and singly charged magnesium clusters consisting of up to 21 atoms, electronic shell closures, binding energies per atom, ionization potentials, and the gap between the highest occupied and the lowest unoccupied molecular orbitals. We have investigated the appearance of the elements of the hcp structure and metallic evolution of the magnesium clusters, as well as the stability of linear chains and rings of magnesium atoms. The results obtained are compared with the available experimental data and the results of other theoretical works.

DOI: 10.1103/PhysRevA.67.063203 PACS number(s): 36.40.Cg, 36.40.Mr, 31.10.+z, 31.15.Ne

## I. INTRODUCTION

Metal clusters have been recognized as new physical objects with their own properties almost two decades ago. This became clear after experimental successes such as the discovery of electronic shell structure in metal clusters [1], observation of plasmon resonances [2–4], formation of singly and doubly charged negative cluster ions [5], and many more. A comprehensive survey of the field can be found in review papers and books; see, e.g., Refs. [6–14].

The electronic shell structure of metal clusters has been discovered in Ref. [1] by the observation of the strong peaks in the mass spectra of sodium clusters. The enhanced stability of some clusters, the so-called magic clusters, was explained by the closure of shells of delocalized electrons. A simple physical model describing electronic shell structure of metal clusters has been developed within the jellium approximation (see, e.g., Ref. [6]) in analogy with the shell model of atomic nuclei (see, e.g., Ref. [15]). The jellium model is very successful for the simple alkali metals (Na, K), for which one electron per atom is delocalized [16–18]. The jellium model electronic shell closures for alkali-metal clusters define the magic numbers $N=8$, 20, 34, 40, 58, 92 that are in a good agreement with the experiment. Note that the jellium model can be generalized by accounting for the collective ion background vibration dynamics [19,20] and can be used as a very appropriate framework for investigating the collision processes involving atomic clusters [21].

Clusters of divalent metals are expected to differ from the jellium model predictions at least at small cluster sizes. In this case, bonding between atoms is expected to have some features of the van der Waals type of bonding, because the electronic shells in the divalent atoms are filled. Thus, clusters of divalent metals are very appropriate to study nonmetal to metal transition, testing different theoretical methodologies and conceptual developments of atomic cluster physics. However, relatively, little work has been done so far on the exploration of the alkali-earth-metal clusters in comparison with that for the alkali-metal clusters; see, e.g., Refs. [6,22], and references therein.

The equilibrium geometries and electronic properties of small magnesium clusters with the number of atoms $N$ up to 4 have been investigated using *ab initio* quantum chemistry methods; see, e.g., Refs. [23–25], and references therein. For cluster size larger than $N=4$, most of the theoretical studies of the magnesium cluster properties have been performed using the pseudopotential approximation for the treatment of inner electrons in a cluster and the density-functional theory (DFT) for the description of outer-shell electrons. The electronic properties, geometry, and stability of small Mg metal clusters with the number of atoms $N\leqslant 7$ have been investigated in Refs. [26,27] using the pseudopotential local-spin-density approximation. The geometrical structure and bonding nature of $Mg_N$ clusters with $N$ up to 13 have been studied in Ref. [28] using the density-functional molecular-dynamics method. The size evolution of bonding in magnesium clusters $Mg_N$ with $N=8-13$, 16, 20 have been studied in Ref. [29] using the local-density approximation that accounts for gradient corrections. Structural and electronic properties of small magnesium clusters ($N\leqslant 13$) were studied in Ref. [30] using a first-principles simulation method in conjunction with the DFT and the generalized gradient-correction approximation for the exchange-correlation functional. It was shown [30] that the metallization in magnesium clusters has a slow and nonmonotonic evolution, although, also jellium-type magic clusters were observed [28,29]. In order to extend such calculations to larger systems, symmetry restricted methods have been developed. The spherically averaged pseudopotential scheme with the local and nonlocal pseudopotentials has been used for the investigation of the electronic structure and shell closures of spherical $Mg_N$ clusters

*Permanent address: Institute of Physics, St Petersburg State University, 198504 St. Petersburg, Petrodvorez, Russia. Email address: lyalin@th.physik.uni-frankfurt.de

†Permanent address: A. F. Ioffe Physical-Technical Institute, 194021 St. Petersburg, Russia. Email address: ilia@th.physik.uni-frankfurt.de

‡Permanent address: A. F. Ioffe Physical-Technical Institute, 194021 St. Petersburg, Russia. Email address: solovyov@th.physik.uni-frankfurt.de

 

up to $N=46$ [31]. The structural and electronic properties of neutral and anionic magnesium clusters $Mg_N$ with $N$ up to 22 have been studied in Refs. [32,33] using gradient-corrected DFT and the Wadt-Hay pseudopotential [34]. All-electron DFT calculations of the energetic and structural properties of neutral magnesium clusters $Mg_N$ ($N=2-22$ and selected clusters up to 309) have been performed in Ref. [35]. The preliminary results of our recent all-electron calculations of the properties of neutral and cationic magnesium clusters with number of atoms $N$ up to 21 have been published in Ref. [36].

Recently, new experimental data for Mg clusters have been obtained, indicating the most intensive peaks in the mass spectra at $N=5$, 10, 15, 18, 20, 25, 28, 30, 35, 40, 47, 56, 59, 62, and 69 [37]. These numbers deviate from the sequence of magic numbers which were obtained for simple alkali-metal clusters, and cannot be reproduced within simple jellium models. This fact was interpreted in Refs. [37,38] within the spherical shell model by diving of the high angular-momentum states down through the states with lower $l$. The mass spectrum of magnesium clusters anions $Mg_N^-$ for $N$ from 3 to 70 has been obtained in Ref. [39]. In the paper cited above, powerful maxima in negative-ion intensity have been observed for $N=4$, 9, 19, 34, 46, 55, and 69, while minima appear for $N=11$, 21, 36, 48, and 57.

In the present work, we investigate the optimized ionic structure and the electronic properties of neutral and singly charged magnesium clusters within the size range $N\leqslant 21$. We calculate binding energies per atom, ionization potentials, and energy gaps between the highest occupied and the lowest unoccupied molecular orbitals. Our calculations are based on *ab initio* theoretical methods invoking the density-functional theory and systematic post–Hartree-Fock many-body theory accounting for all electrons in the system. The results obtained are compared with the available experimental data and the results of other theoretical works.

The atomic system of units, $|e|=m_e=\hbar=1$, has been used throughout the paper, unless other units are indicated.

## II. THEORETICAL METHODS

Our calculations have been performed with the use of the GAUSSIAN 98 software package [40]. We have utilized the $6-311G(d)$ basis set of primitive Gaussian functions to expand the cluster orbitals [40,41].

The cluster geometries have been determined by finding local minima on the multidimensional potential-energy surface for a cluster. We have taken into account all electrons available in the system when computing the potential-energy surface. With increasing cluster size, such calculations become computer-time demanding. In this work, we limit the calculations with the cluster size $N=21$.

The key point of calculations is fixing the starting geometry of the cluster, which could converge during the calculation to a local or to the global minimum. There is no unique way for achieving this goal with GAUSSIAN 98 [41]. In our calculations, we have created the starting geometries empirically, often assuming certain cluster symmetries. Note that during the optimization process, the geometry of the cluster as well as its initial symmetry sometimes change dramatically. All the characteristics of the clusters, which we have calculated and present in the following section, are obtained for the clusters with optimized geometry.

In this work, we concentrate on the systematic exploration of the properties of magnesium clusters using the density-functional theory based on the hybrid Becke-type three-parameter exchange functional [42] paired with the gradient-corrected Lee, Yang, and Parr correlation functional (B3LYP) [43,44], as well as with the gradient-corrected Perdew-Wang 91 correlation functional (B3PW91) [45,46]. The important feature of the density-functional method consists of the fact that it takes into account many-electron correlations via the phenomenological exchange-correlation potential. However, so far, a unique potential, has not been found universally applicable for different systems and conditions. As a result, there are many different parametrizations for the exchange-correlation potential valid for special cases.

Alternatively, we use a direct *ab initio* method for the description of electronic properties of metal clusters, which is based on the consistent post–Hartree-Fock many-body theory [47]. In the present work, we apply the Møller-Plesset perturbation theory of the second and fourth order (MP2) and (MP4), respectively. Based on the fundamental physical principles being free from any phenomenological parameters, this model can be refined by extending the quality of the approximations, while the physical meaning of the effects included is clearly demonstrated. Thus, often such an approach predicts more accurate and reliable characteristics of metal clusters than the density-functional theory.

In the present work, we use both different theoretical schemes for calculations taking advantage of the clear physical meaning and the reliability of the post–Hartree-Fock perturbation theory and the numerical efficiency of the density-functional methods.

## III. NUMERICAL RESULTS AND DISCUSSION

### A. Geometry optimization of $Mg_N$ and $Mg_N^+$ clusters

The optimization of the cluster geometries has been performed with the use of the B3PW91 and B3LYP methods. For small magnesium clusters with number of atoms $N\leqslant 11$, we have also used the *ab initio* MP2 and MP4 methods in addition to density-functional calculations. In the latter case, we have optimized the cluster geometries with the use of the MP2 method and then calculated total energies using MP4 method. With the increase in cluster size, the *ab initio* MP2 and MP4 calculations become more and more computer-time demanding, therefore we have not performed such calculations for magnesium clusters with number of atoms $N\geqslant 12$. The comparison, in detail, of the results obtained by the density-functional and *ab initio* perturbation theory methods as well as their comparison with the results of other works is given below, see Sec. III B. This comparison allows us to conclude that for magnesium clusters, the B3PW91 method is more reliable and accurate in comparison with the B3LYP one.

The results of the cluster geometry optimization for neutral and singly charged magnesium clusters consisting of up

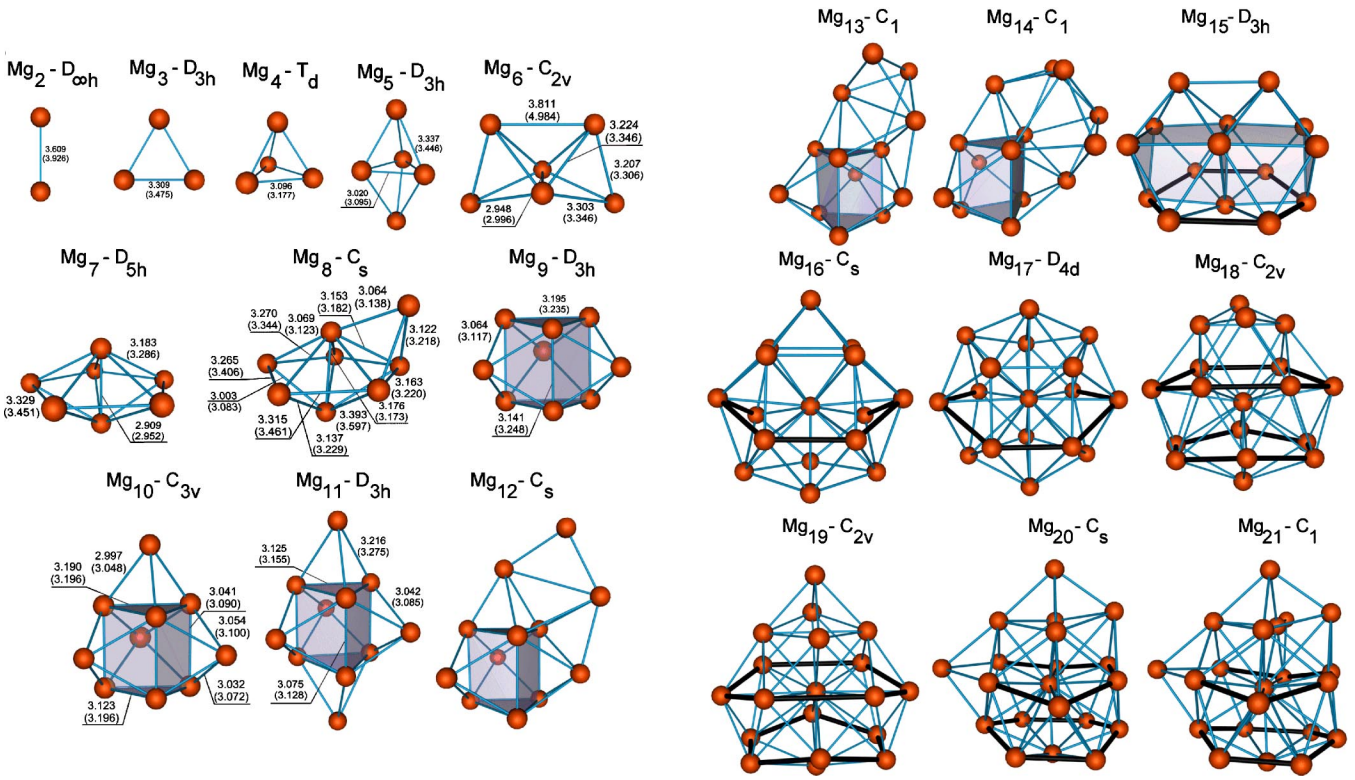


FIG. 1. Optimized geometries of the neutral magnesium clusters $Mg_2$-$Mg_{21}$ calculated in the B3PW91 approximation. The interatomic distances are given in angstroms. The values in brackets correspond to the B3LYP results. The label above each cluster image indicates the point symmetry group of the cluster.

to 21 atoms are shown in Figs. 1 and 2, respectively.

Magnesium clusters possess various isomer forms, number of which increases dramatically with increasing cluster size. In Figs. 1 and 2, we present only the lowest-energy configurations optimized by the B3PW91 method. The interatomic distances are given in angstroms. The values in brackets correspond to the interatomic distances obtained by the B3LYP method.

Figure 1 shows that the neutral magnesium clusters form the compact structures, maximizing the coordination number. The $Mg_2$ dimer is weakly bound possessing the binding energy per atom 0.039 eV/atom and the bond length 3.609 Å, which is in a good agreement with the experimental results of Ref. [48], where the values are 0.025 eV/atom for the binding energy and 3.89 Å for the bond length have been reported. The lowest-energy state for $Mg_3$ is the equilateral triangle, and for $Mg_4$ is a regular tetrahedron. As we discuss below, the $Mg_4$ cluster is relatively more stable and compact, as compared to the neighboring clusters. The $Mg_5$ cluster has a structure of slightly elongated triangular bipyramid, while $Mg_6$ consists of three pyramids connected by their faces, $Mg_7$ is a pentagonal bipyramid, and $Mg_8$ is a capped pentagonal bipyramid. These geometrical structures are in a good agreement with the results of Refs. [28,32,33,35].

It is worth noting that the optimized geometry structures for small neutral magnesium clusters differ significantly from those obtained for sodium clusters (see, e.g., Refs. [22,49,50], and references therein). Thus, the optimized sodium clusters with $N \leqslant 6$ have the plane structure. For $Na_6$, both plane and spatial isomers with very close total energies exist. The planar behavior of small sodium clusters has been explained as a result of the successive filling of the $1\sigma$ and $1\pi$ symmetry orbitals by delocalized valence electrons [49], which is fully consistent with the deformed jellium model calculations [18]. Contrary to the small sodium clusters, the magnesium clusters are tridimensional already at $N=4$, forming the structures nearly the same as the van der Waals bonded clusters.

Starting from $Mg_9$, a new element appears in the magnesium cluster structures. This is the six-atom trigonal prism core, which is marked out in Fig. 1. The formation of the trigonal prism plays an important role in the magnesium cluster growth process. Adding an atom to one of the triangular faces of the trigonal prism of the $Mg_9$ cluster results in the $Mg_{10}$ structure, while adding an atom to the remaining triangular face of the prism within the $Mg_{10}$ cluster leads to the structure of $Mg_{11}$, as shown in Fig. 1.

Further growth of the magnesium clusters for $12 \leqslant N \leqslant 14$ leads to the formation of the low-symmetry ground-state cluster. In spite of their low symmetry, all these clusters have the trigonal prism core. The structural rearrangement occurs for the $Mg_{15}$ cluster, which results in the high-symmetry structure of the two connected $Mg_9$ clusters.

Starting from $Mg_{15}$, another motif based on the hexagonal ring structure that is marked out in Fig. 1 dominates the cluster growth. Overall, obtained structures agree with those obtained from Refs. [32,33], where the Wadt-Hay pseudopotential has been used for the treatment of the magnesium

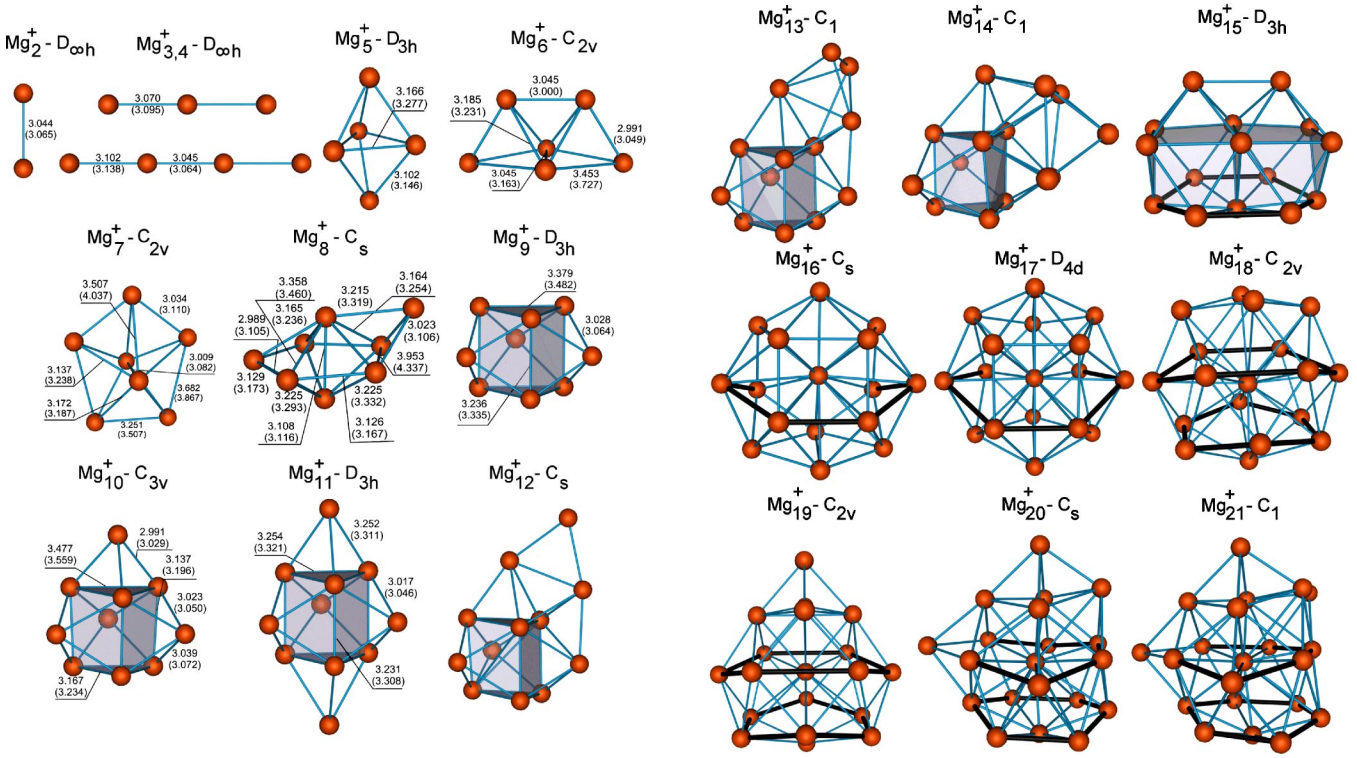


FIG. 2. Same as in Fig. 1, but for singly charged magnesium clusters $Mg_2^+$-$Mg_{21}^+$.

ionic core. However, the most stable structures for $Mg_{13}$, $Mg_{15}$, $Mg_{16}$, $Mg_{19}$, and $Mg_{20}$ clusters obtained in Ref. [35] emerge as higher-energy isomers in our calculations.

It is worth noting that the formation of hexagonal ring for $N=15$ plays an important role in the evolution of the magnesium cluster structure into the bulk lattice. A single deformed hexagonal ring a the common element in the structures of the $Mg_{16}$ and $Mg_{17}$ clusters. For the $Mg_{18-21}$ clusters, two deformed hexagonal rings appear. The hexagonal ring is one of the basic elements of the hexagonal-close-packing (hcp) lattice, as one can see in Fig. 3, in which the primitive cell for the magnesium hcp lattice is presented.

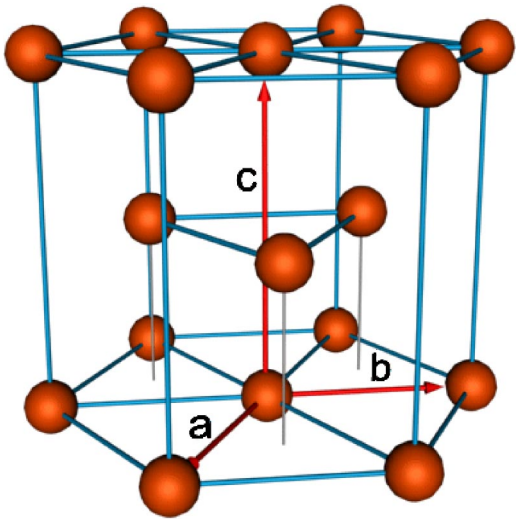


FIG. 3. Primitive cell for magnesium hcp lattice. For bulk magnesium, $a=b=3.21$ Å and $c=5.21$ Å [51].

Vectors **a**, **b**, and **c** in Fig. 3 show the primitive cell axes of the hcp lattice. For bulk magnesium, $a=b=3.21$ Å and $c=5.21$ Å [51]. The fundamental characteristic for the hexagonal close packing of spheres is the value of ratio $c/a$, which is equal to $\sqrt{8/3}\approx 1.633$ for an ideal hcp lattice. The bulk magnesium with $c/a=1.62$ is very close the ideal hcp structure [52]. The distinct three-layered structure of Mg clusters with $N\geqslant 18$ based on the deformed hexagonal rings allows one to determine the averaged values of the primitive axes $\langle c\rangle$ and $\langle a\rangle$. Table I demonstrates that the calculated values $\langle c\rangle$ and $\langle a\rangle$ and their ratio for magnesium clusters with $N\geqslant 18$ are close to the corresponding values for bulk magnesium. However, we stress that the appearance of the hexagonal rings is a necessary but not sufficient condition for the formation of the regular hcp structure.

Figure 2 shows the optimized geometries of singly charged cationic magnesium clusters. The ground-state geometries of the cationic magnesium clusters are not very different from those obtained for the neutral parent clusters with the exception of $Mg_3^+$ and $Mg_4^+$, the equilibrium geometries of which are linear chains. Below, we discuss the stability of the linear-chain isomers for the magnesium clusters (neutral and singly charged) within the size range considered.

In Fig. 4, we present the average bonding distance $\langle d\rangle$ calculated within the B3PW91 approximation for neutral and singly charged magnesium clusters. For calculating the average bonding distance in a cluster, interatomic distances smaller than 4.1 Å have only been taken into account. The

TABLE I. The average values of the primitive axes and their ratio for the hcp lattice element for magnesium clusters with $N \geqslant 18$, calculated within the B3PW91 approximation. Values in brackets correspond to singly charged magnesium clusters.

| | $Mg_{18}$ | $Mg_{19}$ | $Mg_{20}$ | $Mg_{21}$ | Mg bulk [51] |
|---|---|---|---|---|---|
| $\langle c \rangle$ (Å) | 5.08 (5.42) | 5.47 (5.37) | 5.48 (5.23) | 5.56 (5.23) | 5.21 |
| $\langle a \rangle$ (Å) | 3.14 (3.19) | 3.05 (3.22) | 3.20 (3.21) | 3.20 (3.21) | 3.21 |
| $\langle c \rangle / \langle a \rangle$ | 1.62 (1.70) | 1.79 (1.67) | 1.71 (1.63) | 1.74 (1.63) | 1.62 |

bulk limit for the magnesium hcp lattice [51] is indicated in the figure by a horizontal dashed line.

Figure 4 shows how the average bonding distance evolves with increasing cluster size. It is clearly seen that the dependence of the average bonding distance on cluster size has essentially a nonmonotonous oscillatory behavior. For $Mg_2$, the bonding distance calculated within the B3PW91 method is equal to 3.609 Å, which is in a good agreement with the experimental result, 3.891 Å, of Ref. [48]. The appearance of the minima in the size dependence of the average bonding distance shows that $Mg_4$, $Mg_{10}$, and $Mg_{20}$ clusters (8, 20, and 40 valence electrons, respectively) are more tightly packed than their neighbors. This behavior can be interpreted by the influence of electronic shell effects on the geometrical structure of magnesium clusters. It supports the conclusion of Ref. [53] that electronic shell effects can enhance the stability of geometric structures resulting from dense ionic packing.

Additional minimum in the dependence of the average bonding distance on $N$ arises at $N=15$. At this $N$ a considerable rearrangement of the cluster geometry takes place, as it is seen in Fig. 1. Indeed, starting from the $Mg_{15}$ cluster, the three-layered structure based on the hexagonal ring is formed. It is clearly seen in Fig. 4 that for $N \geqslant 15$, the average bonding distance for magnesium clusters approaches the bulk limit.

The evolution of the average bonding distance with cluster size differs for magnesium clusters from that for sodium. For neutral sodium clusters, one can see odd-even oscillations of $\langle d \rangle$ atop its systematic growth and approaching the bulk limit [22]. These features have the quantum origin and arise due to the spin coupling of the delocalized valence electrons. For magnesium clusters, the average bonding distance depends on size nonmonotonically, with minima for the $Mg_4$, $Mg_{10}$, $Mg_{15}$, and $Mg_{20}$ clusters. Such an irregular behavior is induced by both the closure of electronic shells of the delocalized electrons and structural rearrangements.

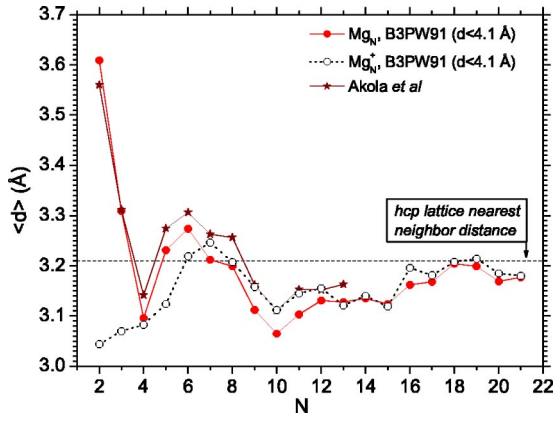


FIG. 4. The average bonding distance as a function of the cluster size for neutral and singly charged magnesium clusters. Stars represent the results of the work by Akola *et al.* [30]. The horizontal dashed line indicates the bulk limit for the hcp lattice [51].

Manifestation of the magic numbers in the dependence of the average bonding distance on cluster size coinciding with the spherical jellium model magic numbers does not imply, however, the rapid metallization of magnesium clusters. To investigate the transition of van der Waals to metal bonding in magnesium clusters, it is necessary to explore, in detail, the evolution of their electronic properties. Below, we perform such an analysis in detail.

Dashed line in Fig. 4 shows the average bonding distance as a function of the cluster size calculated for singly charged magnesium clusters. Figure 4 demonstrates the essential difference in the cluster size dependence of $\langle d \rangle$ for the cationic and neutral magnesium clusters with $N \leqslant 6$. The small cationic magnesium clusters are more compact in comparison with the corresponding neutral clusters. For example, for $Mg_2^+$ the bonding distance is equal to 3.044 Å, which is much less than in the case of $Mg_2$. This phenomenon has a simple physical explanation: the removed electron is taken from the antibonding orbital. The fact that cationic magnesium clusters are more stable than the parent neutral and anionic clusters has been already noted in Ref. [27].

Within the size range $N \geqslant 7$, the average bonding distances for single-charged and neutral magnesium clusters behave similarly. The absolute value of $\langle d \rangle$ for single-charged clusters is slightly larger in this region of $N$.

Figure 4 demonstrates the good agreement of our results with the dependence of $\langle d \rangle$ on $N$ calculated in Ref. [30] for neutral Mg clusters within the size range $N \leqslant 13$.

### B. Binding energy per atom for $Mg_N$ and $Mg_N^+$ clusters

The binding energy per atom for small neutral and singly charged magnesium clusters is defined as follows:

$$E_b/N = E_1 - E_N/N, \tag{1}$$

$$E_b^+/N = [(N-1)E_1 + E_1^+ - E_N^+]/N, \tag{2}$$

where $E_N$ and $E_N^+$ are the energies of a neutral and singly charged $N$-particle atomic cluster, respectively. $E_1$ and $E_1^+$ are the energies of a single magnesium atom and an ion.

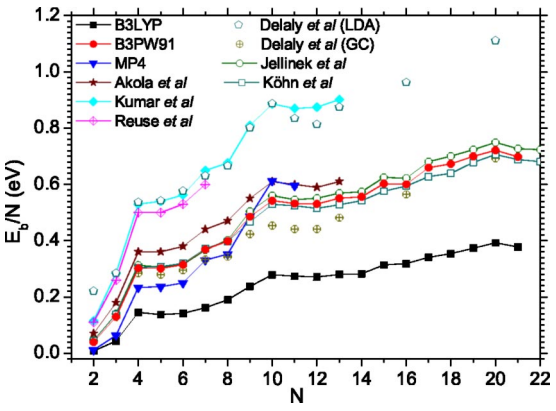


FIG. 5. Binding energy per atom for the most stable neutral magnesium clusters as a function of the cluster size. Squares, circles, and lower triangles represent the binding energies per atom calculated by the B3LYP, B3PW91, and MP4 methods, respectively. Stars, filled rhombuses, and crossed rhombuses show the results of the works by Akola *et al.* [30], Kumar *et al.* [28], and Reuse *et al.* [27], respectively. Open pentagons and crossed circles show the result of Delaly *et al.* [29] obtained with the use of the LDA (local density approximation) and gradient-corrected (GC) LDA methods, respectively. Open circles and open squares show the results of the works by Jellinek and co-workers [32,33] and Köhn *et al.* [35], respectively. The geometries and the point symmetry group of the isomers presented can be found in Sec. III A.

Figures 5 and 6 show the dependence of the binding energy per atom for the most stable neutral and singly charged clusters as a function of the cluster size. The energies of the clusters have been obtained using the B3LYP, B3PW91, and MP4 methods. Calculations of the binding energies have been performed by different theoretical methods and with the use of different exchange-correlation functionals for the sake of comparison of their accuracy and computation efficiency. In Fig. 5, filled rhombus, crossed rhombus, and open pentagons show the result of calculations by Kumar and Car [28], Reuse *et al.* [27], and Delaly *et al.* [29], respectively. These calculations have been performed within the Hohenberg-Kohn-Sham local-density approximation using the Perdew and Zunger [54] parametrization of the Ceperley and Alder

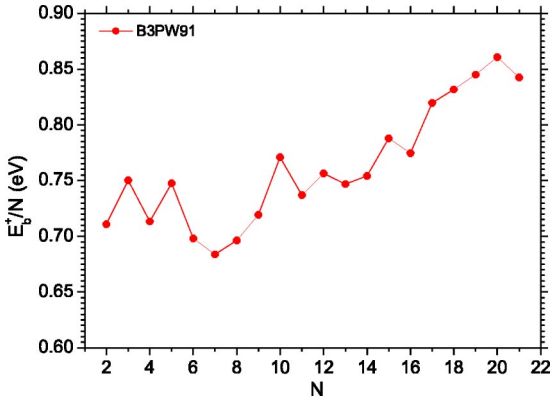


FIG. 6. Same as in Fig. 5, but for singly charged magnesium clusters.

[55] data for the exchange correlations. Crossed circles and stars present the results of Delaly *et al.* [29] and Akola *et al.* [30] derived with the use of the gradient-corrected approximation [56,57] and the Perdew-Burke-Ernzerhof (PBE) parametrization of the gradient-corrected exchange-correlation energy functional [58], respectively. Open circles represent the results by Jellinek and co-workers [32,33], which have been obtained within the DFT with the Becke exchange [42] and the Perdew correlation [56] functionals (BP86). The Ne-like core of the Mg atom was described in Refs. [32,33] by the Wadt-Hay pseudopotential [34]. Open squares show the results by Köhn *et al.* [35] derived from the all-electron DFT employing the BP86 exchange-correlation functional.

Figure 5 shows that, although, the qualitative behavior of the binding energy per atom, calculated within different approaches, is similar, the quantitative discrepancy between the curves is rather considerable. This is a result of a different way of accounting for the gradient corrections to the local-density exchange-correlation interaction within different methods. The gradient corrections have been shown to provide a systematic improvement in the computed properties of magnesium clusters [29]. The difference in the binding energy per atom for neutral magnesium clusters with $N \leqslant 21$ calculated with the use of the gradient-corrected B3LYP and B3PW91 methods reaches 0.35 eV. The reason for this difference is in the different way of accounting for many-electron correlations within the B3LYP and B3PW91 methods. To explore what type of parametrization of the exchange-correlation energy is more reliable for magnesium clusters, we have used the post–Hartree–Fock–Møller-Plesset perturbation theory. This method is free of phenomenological parameters and can be used as a criterion for checking the reliability of various density-functional-theory schemes. The disadvantage of the perturbation-theory approach consists of the fact that it leads to the dramatic growth of the computational costs by increasing the number of electrons in the system in comparison with that for the density-functional-theory calculations. Therefore, we have used the MP4 method only for clusters with the number of atoms, $N \leqslant 11$.

Figure 5 shows that the results of the MP4 theory are in a reasonable agreement with those derived by the B3PW91 method. This comparison demonstrates that for magnesium cluster simulations the B3PW91 method is more reliable than the B3LYP one. Our results derived within the B3PW91 and MP4 approximations are in a reasonable agreement with those from Refs. [29,30] and in a very good agreement with those from Refs. [32,33,35]. It is worth noting that the binding energy of magnesium clusters, obtained in Refs. [32,33] with the use of the pseudopotential for the treatment of the $1s2s1p$ magnesium core electrons, appears to be systematically larger within the range $N \geqslant 10$ than $E_b/N$ obtained in the present work. The difference is, however, negligibly small and averages to about 0.03 eV.

We now discuss the behavior of the binding energy as a function of the cluster size for both neutral and singly charged magnesium clusters. For neutral magnesium clusters, the binding energy per atom increases steadily with the increasing cluster size. The local maxima of $E_b/N$ at $N$

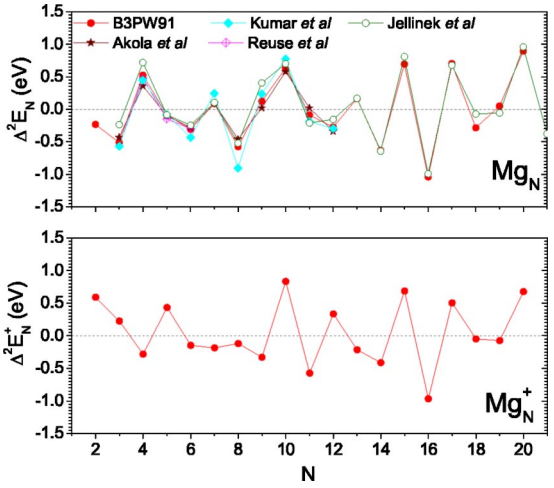


FIG. 7. Second differences of total energy for neutral, $\Delta^2 E_N = E_{N+1} - 2E_N + E_{N-1}$, and singly charged, $\Delta^2 E^+_N = E^+_{N+1} - 2E^+_N + E^+_{N-1}$, magnesium clusters. Filled circles show the B3PW91 results obtained in this work; stars, results obtained by Akola *et al.* [30]; filled rhombuses, results of Kumar *et al.* [28]; crossed rhombuses, results of Reuse *et al.* [27]; and open circles, results of Jellinek and co-workers [32,33].

$=4$, 10, and 20 correspond to the most stable configurations of the magic magnesium clusters possessing $N_{el}=8$, 20, and 40 valence electrons, respectively. This behavior is in agreement with the simple spherical jellium model. The analysis of the second differences of the binding energy (see Fig. 7) confirms this conclusion and gives a hint about the relative stability of the $Mg_7$, $Mg_{13}$, $Mg_{15}$, and $Mg_{17}$ clusters, in addition to the magic clusters $Mg_4$, $Mg_{10}$, and $Mg_{20}$. The additional magic numbers can be explained within the deformed jellium model accounting for spheroidal deformations of the cluster core (see, e.g., Refs. [16–18], and references therein). For a spheroidal jellium cluster, the orbital angular momentum does not remain a good quantum number characterizing the valence electron's energy levels. In this case, the energy levels are characterized by the projection of the angular momentum $\Lambda$ on the principal axis and by the parity of the wave function. Thus, the energy levels with $\Lambda = 0$ are twofold degenerate on the projection of the electron's spin, while those with $\Lambda \neq 0$ are fourfold degenerate both on the projection of the electron spin and on the sign of the projection $\Lambda$ on the principal cluster axis. The deformed jellium clusters having closed electronic subshells possess the enhanced stability. Therefore, in addition to the spherical magic clusters with 8, 20, 40, etc., valence electrons, the deformed jellium clusters with 6, 10, 14, 18, 22, 26, 30, 34, etc., valence electrons turn out to be relatively stable. This fact leads to the following additional magic numbers 3, 5, 7, 9, 11, 13, 15, 17 for the jellium magnesium clusters. Some of these numbers, such as 3, 5, 9, 11, precede or follow the spherical magic numbers 4, 10, 20, and as a result become masked and are not that pronounced in the second differences analysis.

For singly charged magnesium clusters, the binding energy per atom as a function of the cluster size is essentially nonmonotonous. The local maxima of the binding energy for the $Mg_3^+$, $Mg_5^+$, $Mg_{10}^+$, $Mg_{12}^+$, $Mg_{15}^+$, and $Mg_{20}^+$ clusters indicate their enhanced stability. Figure 7 shows the second differences of the total energy for singly charged magnesium clusters. This figure demonstrates the enhanced stability of the mentioned cluster ions and the $Mg_{17}^+$ cluster.

The sequence of magic numbers for singly charged magnesium clusters differs from that for neutral clusters. This happens because singly charged magnesium clusters always possess odd number of valence electrons and, thus, always contain open electronic shells. For neutral magnesium clusters, situations of both close and open electronic shells are possible. The enhanced stability of a Mg-cluster ion arises, when its electronic configuration has one hole in or an extra electron above the filled shells. Thus, the cluster ions $Mg_5^+$, $Mg_{11}^+$, and $Mg_{21}^+$ contain one extra electron over the completed spherical electronic shells, while the clusters $Mg_4^+$, $Mg_{10}^+$, and $Mg_{20}^+$ have a hole in the spherical outer electronic shell. Our results presented in Figs. 6 and 7 demonstrate that the cluster ions $Mg_5^+$, $Mg_{10}^+$, and $Mg_{20}^+$ turn out to be more stable than their neighbors. We note that the alteration of the magic number from $N=4$ for neutral Mg clusters to $N=5$ for Mg cluster ions occurs because the electronic configuration containing an extra electron becomes more favorable for $Mg_5^+$. This is not the case for the $Mg_{10}^+$ and $Mg_{20}^+$ clusters, those outer electronic configurations contain a hole.

The Mg cluster mass spectra have been recorded in Ref. [37], indicating the enhanced stability of the clusters with $N=5$, 10, 15, 18, and 20. In that work, the role of the cluster ionization was not reliably clarified [37] and, thus, the charge state of the clusters was not reliably determined. As a result, the observed magic numbers sequence should be a combination of the magic number sequences for neutral and singly charged cluster ions. Thus, $N=5$ is the ionic magic number, and $N=10$, 15, and 20 are the magic numbers manifesting themselves clearly for both neutral Mg clusters and Mg cluster ions. The second differences are positive and relatively large for $N=13$ (neutral clusters) and $N=12$ (singly charged cluster ions). Possibly, the interplay between neutral clusters and ions make these numbers masked in experiment. The second differences are also positive for $N=7$ for neutral Mg clusters and for $N=3$ for Mg cluster ions, although the enhancement for these numbers have not been experimentally observed. We explain this fact by a possible suppression of the experimental signal in the region of small $N$ and relatively small values of the second differences in the mentioned cases.

The potential-energy surface for a cluster becomes more and more complex with increasing cluster size. The magnesium clusters are not an exception. Figure 8 demonstrates this fact where we present the binding energies per atom calculated for a variety of isomers of neutral magnesium clusters. The corresponding point symmetry groups and the accurate values of the total energies calculated within the B3LYP, B3PW91, and MP4 approximations are presented in Tables II–IV, respectively. Most of the isomer configurations have been obtained using the B3LYP method, while the B3PW91 method has been used for the exploration of the ground-state energy isomers, as well as for the linear and

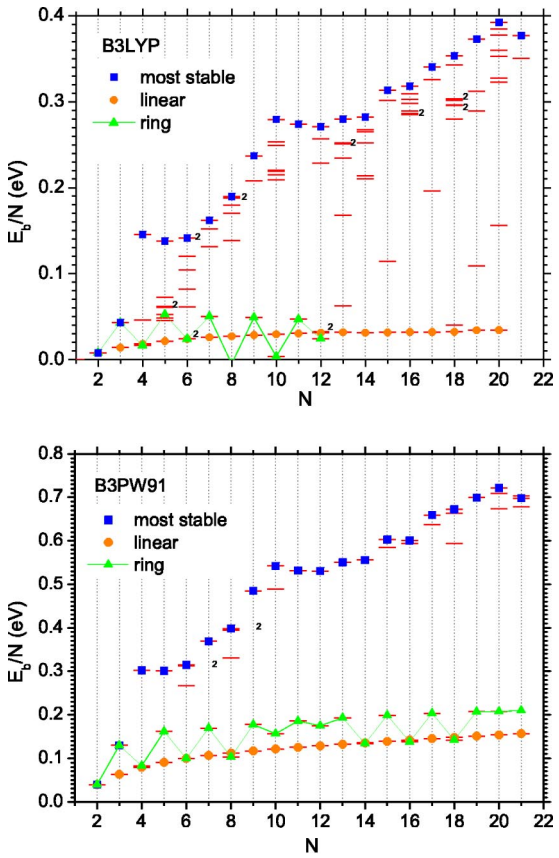


FIG. 8. Binding energy per atom for a variety of isomers of neutral magnesium clusters as a function of the cluster size. The corresponding point symmetry groups and the accurate values of the total energies are presented in Tables II and III. Numbers near some lines show the number of found isomers with the corresponding close energies.

ringlike isomer structures. The MP4 method has been used only for the exploration of the ground-state energy isomers within the range $N \leqslant 11$.

Squares in Fig. 8 correspond to the most stable clusters possessing the minimal total energy. Among the variety of isomers, presented in Fig. 8, we mark certain groups of isomers with fixed symmetry. So, circles present the linear chains ($D_{\infty h}$ point symmetry group) and the upper triangles correspond to the rings of $N$ atoms ($D_{Nh}$ point symmetry group). It is an interesting fact that among the multitude of the isomers of neutral magnesium clusters, the linear chains and rings always possess the positive binding energy. We pay special attention to these structures because of their possible applications in nanotechnology. Under special experimental conditions, one can expect the stability of one-atom wide quantum wires of magnesium. For example, it is interesting to investigate the properties of such isomers deposited on a substrate. The interaction of the linear isomers with the surface can prevent them from the relaxation to more stable three-dimensional structures of free clusters. The linear chains and rings of atoms are also very interesting from the theoretical point of view, because with their help one can investigate the transition from one- to two-dimensional structures. For linear chains, the binding energy per atom increases slowly with the increase in the number of atoms, while in the case of rings the value of $E_b/N$ has the prominent odd-even oscillatory behavior.

This behavior arises as a result of successive filling of the $\sigma$- and $\pi$-symmetry orbitals by valence electrons in magnesium linear chains and rings. Indeed, because of its symmetry the one-dimensional linear chain of $N$ magnesium atoms has the following configuration of valence electrons: $1\sigma^2$, $2\sigma^2$, $3\sigma^2$, $\ldots$, $N\sigma^2$. Therefore, for any $N$ it has the closed electronic shell structure. This fact explains the monotonous growth with $N$ of the linear chain binding energy and its relative saturation to the region $N>10$.

The molecular orbitals for the structure of the ring type have to be aligned with the plane of the ring. Such orbitals are fourfold degenerate due to symmetry reasons. The $Mg_2$ dimer has four valence electrons that occupy spherically shaped $1\sigma^2$ and prolatelike $2\sigma^2$ orbitals. The $Mg_3$ trimer has six valence electrons, two of them occupy $1\sigma^2$ state, while the remaining four electrons fill the fourfold degenerate $1\pi^4$ orbital, aligned with the plane of the trimer. On increasing the number of magnesium atoms in the ring, the valence electrons continue to occupy fourfold degenerate orbitals aligned with the plane of the ring. Therefore, in the magnesium ringlike isomers with an odd number of atoms, all electronic shells are closed, while the isomers with an even number of atoms have the open electronic shell. This fact results in the enhanced stability of the magnesium rings with an odd number of atoms $N=3,5,7,9,\ldots$, etc., and explains the odd-even oscillatory behavior of the binding energy for the magnesium rings.

### C. Ionization potentials and HOMO-LUMO (highest occupied molecular orbital and lowest unoccupied molecular orbital) gaps

Let us now consider how the ionization potential of magnesium clusters evolves with the increasing cluster size. The ionization potential of a cluster $V_i$ is equal to the difference between the energies of the corresponding cluster ion and the neutral cluster, $V_i = E_N^+ - E_N$. Figure 9 shows the dependence of the adiabatic $V_i^{adiab}$ (i.e., the geometry relaxation of the ionized cluster is taken into account) and vertical $V_i^{vert}$ (i.e., the cluster geometry is frozen during the ionization process) ionization potential on $N$. We compare our results derived by the B3PW91 method with theoretical data from Refs. [30,27] and with the bulk limit, $V_i^{bulk}=3.64$ eV, taken from Ref. [51].

Both the vertical and adiabatic ionization potentials evolve nonmonotonously with the increasing cluster size. Figure 9 shows that ionization potential of magnesium clusters steadily but rather slowly decreases towards the bulk limit. This evolution is neither a rapid nor a monotonous process. In order to exclude the influence of the cluster geometry rearrangement, we first consider the vertical ionization potential. The size dependence of the vertical ionization potential has a prominent maximum at $N=4$ followed by a sharp decrease. Such a behavior of the ionization potential is typical for the jellium model, predicting maxima in the size dependence of the ionization potential at the magic numbers

TABLE II. Total energies and the point symmetry groups for a variety of isomers of neutral magnesium clusters. Calculations have been done by the B3LYP method.

| $N$ | Point group | Energy (a.u.) | $N$ | Point group | Energy (a.u.) | $N$ | Point group | Energy (a.u.) |
|---|---|---|---|---|---|---|---|---|
| 1 | | −200.0931 | 9 | $D_{\infty h}$ | −1800.8472 | 16 | $d.C_s$ | −3201.6766 |
| 2 | $D_{\infty h}$ | −400.1868 | 10 | $C_{3v}$ | −2001.0336 | | $c.C_s$ | −3201.6713 |
| 3 | $D_{3h}$ | −600.2840 | | $C_{4v}$ | −2001.0239 | | $b.C_1$ | −3201.6673 |
| | $D_{\infty h}$ | −600.2807 | | $T_d$ | −2001.0225 | | $a.C_1$ | −3201.6646 |
| 4 | $T_d$ | −800.3938 | | $C_1$ | −2001.0120 | | $T_d$ | −3201.6594 |
| | $D_{2h}$ | −800.3792 | | $D_{3h}$ | −2001.0114 | | $a.C_s$ | −3201.6579 |
| | $D_{\infty h}$ | −800.3750 | | $C_{2v}$ | −2001.0098 | | $b.C_s$ | −3201.6572 |
| | $D_{4h}$ | −800.3748 | | $D_{4d}$ | −2001.0078 | | $D_{\infty h}$ | −3201.5082 |
| 5 | $D_{3h}$ | −1000.4907 | | $D_{\infty h}$ | −2000.9417 | 17 | $D_{4d}$ | −3401.7953 |
| | $C_{4v}$ | −1000.4787 | | $D_{10h}$ | −2000.9322 | | $C_s$ | −3401.7861 |
| | $T_d$ | −1000.4768 | 11 | $D_{3h}$ | −2201.1348 | | $D_{3h}$ | −3401.7052 |
| | $C_{2v}$ | −1000.4766 | | $D_{11h}$ | −2201.0430 | | $D_{\infty h}$ | −3401.6026 |
| | $D_{5h}$ | −1000.4751 | | $D_{\infty h}$ | −2201.0362 | 18 | $b.C_{2v}$ | −3601.9095 |
| | $D_{2D}$ | −1000.4743 | 12 | $a.C_s$ | −2401.2366 | | $c.C_s$ | −3601.9026 |
| | $D_{2h}$ | −1000.4738 | | $b.C_s$ | −2401.2304 | | $C_2$ | −3601.8764 |
| | $D_{\infty h}$ | −1000.4694 | | $C_{2v}$ | −2401.2178 | | $b.C_s$ | −3601.8752 |
| 6 | $C_{2v}$ | −1200.5898 | | $D_{6h}$ | −2401.1313 | | $a.C_s$ | −3601.8716 |
| | $D_{2h}$ | −1200.5897 | | $D_{\infty h}$ | −2401.1308 | | $a.C_{2v}$ | −3601.8711 |
| | $D_{4h}$ | −1200.5851 | | $D_{12h}$ | −2401.1278 | | $D_{5h}$ | −3601.8608 |
| | $C_{5v}$ | −1200.5815 | 13 | $b.C_1$ | −2601.3438 | | $D_{6h}$ | −3601.7022 |
| | $D_{3h}$ | −1200.5765 | | $C_S$ | −2601.3308 | | $D_{\infty h}$ | −3601.6970 |
| | $O_h$ | −1200.5720 | | $a.C_1$ | −2601.3302 | 19 | $C_{2v}$ | −3802.0292 |
| | $D_{6h}$ | −1200.5639 | | $C_{3v}$ | −2601.3221 | | $C_{3v}$ | −3801.9867 |
| | $D_{\infty h}$ | −1200.5638 | | $I_h$ | −2601.2904 | | $D_{5h}$ | −3801.9706 |
| 7 | $D_{5h}$ | −1400.6933 | | $D_{6h}$ | −2601.2401 | | $D_{6h}$ | −3801.8449 |
| | $C_3$ | −1400.6908 | | $D_{\infty h}$ | −2601.2253 | | $D_{\infty h}$ | −3801.7925 |
| | $C_{3v}$ | −1400.6854 | 14 | $C_1$ | −2801.4485 | 20 | $C_s$ | −4002.1503 |
| | $D_{7h}$ | −1400.6645 | | $b.C_{3v}$ | −2801.4397 | | $C_1$ | −4002.1444 |
| | $D_{\infty h}$ | −1400.6583 | | $C_s$ | −2801.4407 | | $d.C_{2v}$ | −4002.1392 |
| 8 | $a.C_{2v}$ | −1600.7999 | | $C_{2v}$ | −2801.4328 | | $c.C_{2v}$ | −4002.1263 |
| | $C_s$ | −1600.7976 | | $O_h$ | −2801.4115 | | $b.C_{2v}$ | −4002.1212 |
| | $b.C_{2v}$ | −1600.7948 | | $a.C_{3v}$ | −2801.4134 | | $T_d$ | −4002.1026 |
| | $T_d$ | −1600.7854 | | $D_{\infty h}$ | −2801.3194 | | $a.C_{2v}$ | −4002.0990 |
| | $D_{\infty h}$ | −1600.7527 | 15 | $D_{3h}$ | −3001.5692 | | $D_{6h}$ | −4001.9764 |
| 9 | $D_{3h}$ | −1800.9162 | | $C_s$ | −3001.5627 | | $D_{\infty h}$ | −4001.8870 |
| | $C_{3v}$ | −1800.9064 | | $D_{6h}$ | −3001.4594 | 21 | $C_1$ | −4202.2460 |
| | $D_{9h}$ | −1800.8540 | | $D_{\infty h}$ | −3001.4138 | | $C_{2v}$ | −4202.2255 |

corresponding to the clusters with closed electronic shells. Our data are in a good agreement with the results of Refs. [27,33], but contradict those reported in Ref. [30] for the $Mg_3$ and $Mg_4$ clusters. In Ref. [30], the appearance of the deep minimum in vertical ionization potential at $N=4$ was explained as a result of a stronger charge delocalization in the $Mg_4$ cluster in comparison with its neighbors.

We note that the peculiarities in the ionization potential dependence on $N$ correlate with the magic numbers that appear for the singly charged magnesium clusters. Indeed, the minima in $V_i^{vert}$ correspond to the maxima in $E_b^+/N$ for Mg cluster ions (see Fig. 6). This fact has a simple explanation. The ionization potential of a cluster is equal to the difference between the energies of the corresponding cluster ion and the neutral cluster. For neutral Mg clusters, the binding energy as a function of $N$ increases steadily with the increase in cluster size, while for Mg cluster ions—irregularly. Thus, their difference mimics all the irregularities that appear in the binding-energy dependence on $N$ for singly charged magnesium clusters.

For $N \geqslant 6$, the vertical ionization potential changes slowly with increasing cluster size. This process is characterized by the irregularities that originate due to the influence of the cluster geometry on the jellium-type electronic structure of Mg clusters.

Indeed, the shape of a jellium cluster is defined by its electronic structure. Thus, the closed-shell jellium clusters are spherical, while clusters with open electronic shells are

TABLE III. Same as Table II, but for the P3PW91 method.

| *N* | Point group | Energy (a.u.) | *N* | Point group | Energy (a.u.) |
|---|---|---|---|---|---|
| 1 | | −200.0379 | 14 | $C_1$ | −2800.8170 |
| 2 | $D_{\infty h}$ | −400.0788 | | $D_{\infty h}$ | −2800.6007 |
| 3 | $D_{3h}$ | −600.1281 | | $D_{14h}$ | −2800.5997 |
| | $D_{\infty h}$ | −600.1207 | 15 | $D_{3h}$ | −3000.9013 |
| 4 | $T_d$ | −800.1962 | | $C_s$ | −3000.8914 |
| | $D_{4h}$ | −800.1638 | | $D_{15h}$ | −3000.6786 |
| | $D_{\infty h}$ | −800.1633 | | $D_{\infty h}$ | −3000.6453 |
| 5 | $D_{3h}$ | −1000.2450 | 16 | $d.C_s$ | −3200.9600 |
| | $D_{5h}$ | −1000.2193 | | $c.C_s$ | −3200.9560 |
| | $D_{\infty h}$ | −1000.2063 | | $D_{\infty h}$ | −3200.6902 |
| 6 | $C_{2v}$ | −1200.2970 | | $D_{16h}$ | −3200.6880 |
| | $D_{2h}$ | −1200.2966 | 17 | $D_{4d}$ | −3401.0569 |
| | $C_{5v}$ | −1200.2865 | | $C_s$ | −3401.0428 |
| | $D_{6h}$ | −1200.2495 | | $D_{17h}$ | −3400.7719 |
| | $D_{\infty h}$ | −1200.2495 | | $D_{\infty h}$ | −3400.7353 |
| 7 | $D_{5h}$ | −1400.3604 | 18 | $b.C_{2v}$ | −3601.1279 |
| | $D_{7h}$ | −1400.3091 | | $c.C_s$ | −3601.1221 |
| | $D_{\infty h}$ | −1400.2928 | | $b.C_s$ | −3601.0756 |
| 8 | $C_s$ | −1600.4205 | | $D_{\infty h}$ | −3600.7806 |
| | $a.C_{2v}$ | −1600.4193 | | $D_{18h}$ | −3600.7766 |
| | $T_d$ | −1600.4005 | 19 | $C_{2v}$ | −3801.2093 |
| | $D_{\infty h}$ | −1600.3364 | | $D_{19h}$ | −3800.8653 |
| | $D_{8h}$ | −1600.3335 | | $D_{\infty h}$ | −3800.8260 |
| 9 | $D_{3h}$ | −1800.5018 | 20 | $C_s$ | −4001.2889 |
| | $D_{9h}$ | −1800.4000 | | $C_1$ | −4001.2801 |
| | $D_{\infty h}$ | −1800.3800 | | $b.C_{2v}$ | −4001.2539 |
| 10 | $C_{3v}$ | −2000.5786 | | $D_{20h}$ | −4000.9111 |
| | $T_d$ | −2000.5590 | | $D_{\infty h}$ | −4000.8716 |
| | $D_{10h}$ | −2000.4367 | 21 | $C_1$ | −4201.3356 |
| | $D_{\infty h}$ | −2000.4238 | | $C_{2v}$ | −4201.3201 |
| 11 | $D_{3h}$ | −2200.6322 | | | |
| | $D_{11h}$ | −2200.4923 | | | |
| | $D_{\infty h}$ | −2200.4678 | | | |
| 12 | $a.C_s$ | −2400.6891 | | | |
| | $D_{12h}$ | −2400.5321 | | | |
| | $D_{\infty h}$ | −2400.5119 | | | |
| 13 | $b.C_1$ | −2600.7561 | | | |
| | $D_{13h}$ | −2600.5853 | | | |
| | $D_{\infty h}$ | −2600.5562 | | | |

deformed due to the Jahn-Teller distortions. The jellium picture works fairly well for sodium clusters. The ionization potential of sodium clusters drops rapidly and systematically at the electronic shell closures. The *N*-dependence of the ionization potential has prominent, regular odd-even oscillations (see, e.g., [18,22] and references therein). Magnesium clusters are different. As discussed in Sec. III A, the evolution of the Mg cluster geometry is closely connected with the formation of elements of the hcp lattice cell. Although, the electronic shell effects clearly manifest themselves in the formation of the Mg cluster geometry, they do not determine it completely. In other words, there is an interplay of the jellium and the hcp lattice factors in the formation of the Mg cluster geometry and the electronic properties such as the binding energy and the ionization potential.

TABLE IV. Same as Table II, but for the MP2 and MP4 methods.

| *N* | Point group | MP2 Energy (a.u.) | MP4 Energy (a.u.) |
|---|---|---|---|
| 1 | | −199.6286 | −199.6381 |
| 2 | $D_{\infty h}$ | −399.2579 | −399.2771 |
| 3 | $D_{3h}$ | −598.8917 | −598.9213 |
| 4 | $T_d$ | −798.5514 | −798.5868 |
| 5 | $D_{3h}$ | −998.1896 | −998.2340 |
| 6 | $C_{2v}$ | −1197.8314 | −1197.8842 |
| 7 | $D_{5h}$ | −1397.4974 | −1397.5518 |
| 8 | $C_s$ | −1597.1508 | −1597.2136 |
| 9 | $D_{3h}$ | −1796.8374 | −1796.9041 |
| 10 | $C_{3v}$ | −1996.5281 | −1996.6062 |
| 11 | $D_{3h}$ | −2196.1701 | −2196.2599 |
| 12 | $a.C_s$ | −2395.8248 | |

The adiabatic ionization potential dependence that is shown in Fig. 9 exhibits qualitatively the same behavior as the vertical one, however, has more pronounced irregularities due to geometry rearrangements of the ionized clusters.

Figure 10 shows the gap $E_g$ between the highest occupied and the lowest unoccupied molecular orbitals (HOMO-

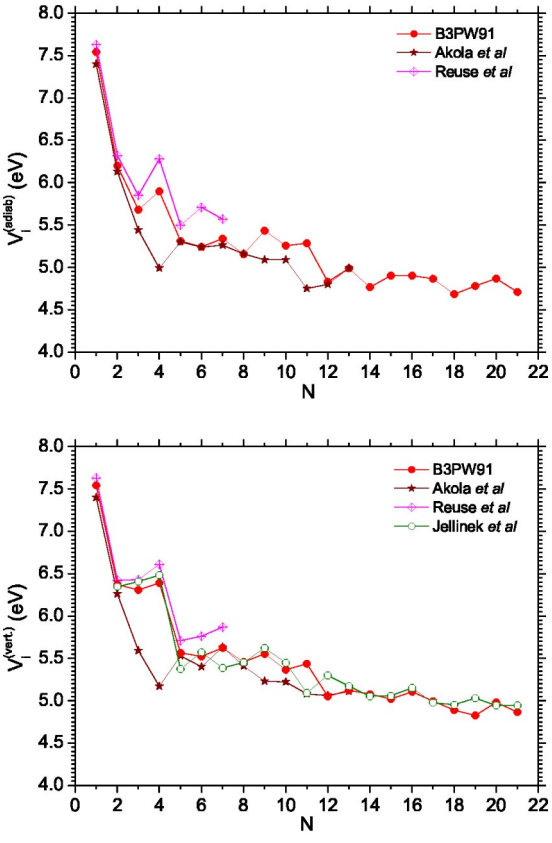


FIG. 9. Adiabatic ($V_i^{adiab}$) and vertical ($V_i^{vert}$) ionization potential for small magnesium clusters. Stars, crossed rhombuses, and open circles show the result of the work of Akola *et al.* [30], Reuse *et al.* [27], and Jellinek and Acioli [33], respectively.

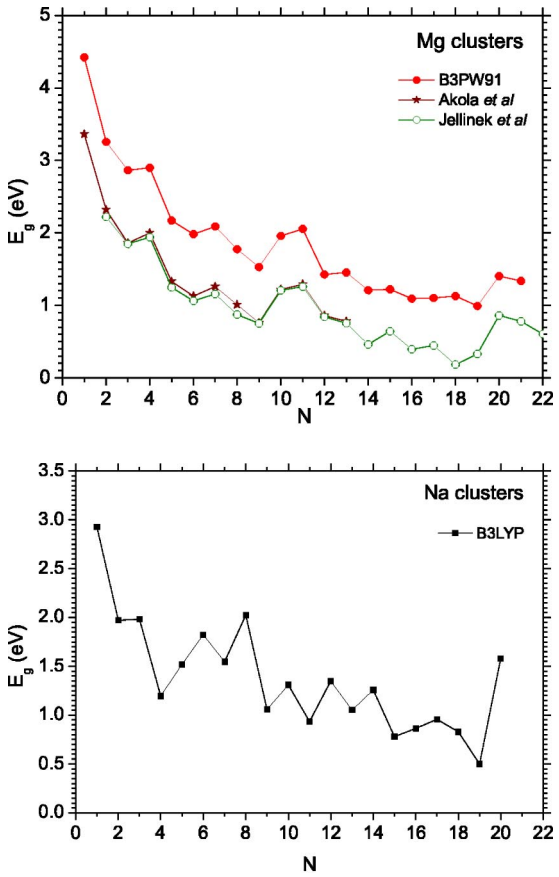


FIG. 10. Gap between the highest occupied and the lowest unoccupied eigenstates for the Mg and Na clusters as a function of the cluster size. Circles and squares represent the HOMO-LUMO gap calculated by the B3PW91 and the B3LYP methods, respectively. Stars and open circles show the results of the work by Akola *et al.* [30] and Jellinek and Acioli [33].

LUMO gap) for the Mg clusters as a function of the cluster size. For the sake of comparison, we have also calculated the HOMO-LUMO gap for the Na clusters and present it in Fig. 10. Calculations have been performed using the B3PW91 and B3PLYP methods. The geometries of neutral sodium clusters have been taken from Ref. [22]. We also compare our results with those presented in Refs. [30,33].

The size dependence of $E_g$ for neutral sodium clusters has an oscillatory behavior with local maxima at $N=6$, 8, 10, 14, and 20. These maxima correspond to the electronic shell closures in full accordance with the deformed jellium model. The local maximum in the size dependence of $E_g$ at $N=12$ and the shift of the local maximum from $N=18$ to $N=17$ are the consequences of triaxial deformations [22]. Thus, the triaxial deformation leads to the splitting of the fourfold degenerate highest occupied orbital into two twofold degenerate orbitals. As a result, the additional shell closure at the $N_{el}=12$ appears.

For Mg clusters, the evolution of the HOMO-LUMO gap with the increase in cluster size differs from that for Na clusters. The gap $E_g$ calculated for magnesium clusters shows the oscillatory behavior accompanied by a gradual decrease in the absolute value. Maxima in this dependence at $N=4$, 10, and 20 correspond to the magic numbers of the spherical jellium model ($N_{el}=8$, 20, and 40, respectively). A similar feature also does exist for Na clusters at $N=8$ and 20. Additional variation of $E_g$ appears both due the subshell closures and the cluster structural rearrangements.

The HOMO-LUMO gap calculated for magnesium clusters in our work with the use of the B3PW91 method appears to be systematically higher if compared with that of Ref. [33] in which the BP86 exchange-correlation functional has been used. Such a discrepancy arises because the pure DFT methods, not accounting explicitly for any Hartree-Fock exchange, tend to give smaller HOMO-LUMO gaps than those obtained by hybrid methods such as B3PW91 [41]. However, the qualitative behavior of the $E_g$ calculated within different approaches is very similar, as it is seen from Fig. 10.

We note that the HOMO-LUMO gap remains rather large even for the clusters with $N \geqslant 15$, possessing geometrical structures with incipient elements of the hcp lattice of the bulk Mg. This fact confirms the conclusion on the slow and nonmonotonous evolution of metallic properties in Mg clusters.

## IV. CONCLUSION

The optimized geometries and electronic properties of neutral and singly charged magnesium clusters consisting of up to 21 atoms have been investigated using the B3PW91, B3LYP, and MP4 methods accounting for all electrons in the system. The detailed comparison of the results of the phenomenological B3PW91 and B3LYP density-functional methods with the results of the systematic *ab initio* post–Hartree-Fock many-body theory leads us to the conclusion that the B3PW91 method is more reliable for Mg cluster simulations than the B3LYP one.

We have investigated the size evolution of the Mg cluster geometry. It has been shown that starting from $Mg_{15}$, the hexagonal ring structure determines the cluster growth. This ring is one of the basic elements of the hcp lattice for the bulk magnesium.

We have investigated the electronic properties of magnesium clusters. It has been shown that the electronic shell effects and jelliumlike behavior clearly manifest themselves in the formation of geometrical properties, however, the shell effects do not determine the geometry of Mg clusters completely. We have demonstrated that due to the interplay of the jellium and the hcp lattice factors, the electronic properties of magnesium clusters possess irregularities which cannot be explained within the simple jellium model. It has been shown that the metallic evolution of magnesium clusters is slow and nonmonotonous process.

The results of this work can be extended in various directions. One can use similar methods to study the structure and properties of various types of clusters. It is interesting to extend calculations towards larger cluster sizes and to perform more advanced comparison of model and *ab initio* ap-

proaches. A lot of novel problems arise, while considering collisions and electron excitations in the clusters with optimized geometries [21]. These and many more other problems on atomic cluster physics can be handled with the use of methods considered in our work.

**ACKNOWLEDGMENTS**

The authors acknowledge support from the Alexander von Humboldt Foundation, RFBR (Grant No. 03-02-16415-A), and the Russian Academy of Sciences (Grant No. 44).

[1] W.D. Knight, K. Clemenger, W.A. de Heer, W.A. Saunders, M.Y. Chou, and M.L. Cohen, Phys. Rev. Lett. **52**, 2141 (1984).
[2] C. Bréchignac, Ph. Cahuzac, F. Carlier, and J. Leygnier, Chem. Phys. Lett. **164**, 433 (1989).
[3] K. Selby, M. Vollmer, J. Masui, V. Kresin, W.A. de Heer, and W.D. Knight, Phys. Rev. B **40**, 5417 (1989).
[4] K. Selby, V. Kresin, J. Masui, M. Vollmer, W.A. de Heer, A. Scheidemann, and W.D. Knight, Phys. Rev. B **43**, 4565 (1991).
[5] A. Herlert, S. Krückeberg, L. Schweikhard, M. Vogel, and C. Walther, Phys. Scr. **T80**, 200 (1999)
[6] *Metal Clusters*, edited by W. Ekardt (Wiley, New York, 1999).
[7] *Atomic Clusters and Nanoparticles*, Proceedings of the Les Houches Session LXXIII, Les Houches, 2000, edited by C. Guet, P. Hobza, F. Spiegelman, and F. David (EDP Sciences, Springer-Verlag, Berlin, 2001).
[8] W.A. de Heer, Rev. Mod. Phys. **65**, 611 (1993).
[9] M. Brack, Rev. Mod. Phys. **65**, 677 (1993).
[10] C. Bréchignac, J.P. Connerade, J. Phys. B **27**, 3795 (1994).
[11] *Clusters of Atoms and Molecules, Theory, Experiment and Clusters of Atoms*, edited by H. Haberland, Springer Series in Chemical Physics Vol. 52 (Springer, Berlin, 1994).
[12] U. Näher, S. Bjørnholm, S. Frauendorf, F. Garcias, and C. Guet, Phys. Rep. **285**, 245 (1997).
[13] *Theory of Atomic and Molecular Clusters. With a Glimpse at Experiments*, edited by J. Jellinek, Springer Series in Cluster Physics (Springer, Berlin, 1999).
[14] *Meal Clusters at Surfaces. Structure, Quantum Properties, Physical Chemistry*, edited by K-H. Meiwes-Broer, Springer Series in Cluster Physics (Springer, Berlin, 1999).
[15] J.M. Eisenberg and W. Greiner, *Collective and Particle Models*, Nuclear Theory Vol. 1. (North-Holland, Amsterdam, 1985).
[16] A.G. Lyalin, S.K. Semenov, A.V. Solov'yov, N.A. Cherepkov, and W. Greiner, J. Phys. B **33**, 3653 (2000).
[17] A.G. Lyalin, S.K. Semenov, A.V. Solov'yov, N.A. Cherepkov, J.-P. Connerade, and W. Greiner, J. Chin. Chem. Soc. (Taipei) **48**, 419 (2001).
[18] A. Matveentsev, A. Lyalin, Il. A. Solov'yov, A. V. Solov'yov, and W. Greiner, Int. J. Mod. Phys. E **12**, 81 (2003); e-print physics/0207085.
[19] L.G. Gerchikov, A.V. Solov'yov, and W. Greiner, Int. J. Mod. Phys. E **8**, 289 (1999).
[20] L.G. Gerchikov, A.N. Ipatov, A.V. Solov'yov, and W. Greiner, J. Phys. B **33**, 4905 (2000).
[21] A.V. Solov'yov, in *Atomic Clusters and Nanoparticles* (Ref. [7]).
[22] Il.A. Solov'yov, A.V. Solov'yov, and W. Greiner, Phys. Rev. A **65**, 053203 (2002).
[23] T.J. Lee, A.P. Rendell, and P.R. Taylor, J. Chem. Phys. **93**, 6636 (1990).
[24] W. Klopper and J. Almlöf, J. Chem. Phys. **99**, 5167 (1993).
[25] C.W. Bauschlicher, Jr. and H. Partridge, Chem. Phys. Lett. **300**, 364 (1999).
[26] F. Reuse, S.N. Khanna, V. de Coulon, and J. Buttet, Phys. Rev. B **39**, 12 911 (1989).
[27] F. Reuse, S.N. Khanna, V. de Coulon, and J. Buttet, Phys. Rev. B **41**, 11 743 (1990).
[28] V. Kumar and R. Car, Phys. Rev. B **44**, 8243 (1991).
[29] P. Delaly, P. Ballone, and J. Buttet, Phys. Rev. B **45**, 3838 (1992).
[30] J. Akola, K. Rytkönen, and M. Manninen, Eur. Phys. J. D **16**, 21 (2001).
[31] Li. Serra, P.-G. Reinhard, and E. Suraud, Eur. Phys. J. D **18**, 327 (2002).
[32] P.H. Acioli and J. Jellinek, Phys. Rev. Lett. **89**, 213402 (2002).
[33] J. Jellinek and P.H. Acioli, J. Phys. Chem. A **106**, 10 919 (2002).
[34] W.R. Wadt and P.J. Hey, J. Chem. Phys. **82**, 284 (1985).
[35] A. Köhn, F. Weigend, and R. Ahlrichs, Phys. Chem. Chem. Phys. **3**, 711 (2001).
[36] A. Lyalin, Il.A. Solov'yov, A.V. Solov'yov, and W. Greiner, e-print physics/0211027.
[37] Th. Diederich, T. Döppner, J. Braune, J. Tiggesbäumker, and K.-H. Meiwes-Broer, Phys. Rev. Lett. **86**, 4807 (2001).
[38] T. Döppner, T. Diederich, J. Tiggesbäumker, and K.-H. Meiwes-Broer, Eur. Phys. J. D **16**, 13 (2001).
[39] O.C. Thomas, W. Zheng, S. Xu, and K.H. Bowen, Phys. Rev. Lett. **89**, 213403 (2002).
[40] M.J. Frisch *et al.*, computer code GAUSSIAN 98, Rev. A. 9 (Gaussian Inc., Pittsburgh, PA, 1998).
[41] James B. Foresman, and Æleen Frisch, *Exploring Chemistry with Electronic Structure Methods* (Gaussian Inc., Pittsburgh, PA, 1996).
[42] A.D. Becke, Phys. Rev. A **38**, 3098 (1988).
[43] C. Lee, W. Yang, and R.G. Parr, Phys. Rev. B **37**, 785 (1988).
[44] R.G. Parr, and W. Yang, *Density-Functional Theory of Atoms and Molecules* (Oxford University Press, Oxford, 1989).
[45] J.P. Perdew, in *Electronic Structure of Solids '91*, edited by P. Ziesche, and H. Eschrig (Akademie Verlag, Berlin, 1991), p. 11.
[46] K. Burke, J.P. Perdew, and Y. Wang, in *Electronic Density Functional Theory: Recent Progress and New Directions*, edited by J.F. Dobson, G. Vignale, and M.P. Das (Plenum, New York, 1998).
[47] C. Møller and M.S. Plesset, Phys. Rev. **46**, 618 (1934).
[48] K.P. Huber and G. Herzberg, *Molecular Spectra and Molecular Structure. IV. Constants of Diatomic Molecules* (Van Nostrand Reinhold, New York, 1979).
[49] J.L. Martins, J. Buttet, and R. Car, Phys. Rev. B **31**, 1804 (1985).

[50] V. Bonačić-Koutecký, P. Fantucci, and J. Koutecký, Phys. Rev. B **37**, 4369 (1988).
[51] N.W. Ashcroft and N.D. Mermin, *Solid State Physics* (Saunders College Publishing, New York, 1976).
[52] C. Kittel, *Introduction to Solid State Physics*, 7th ed. (J. Wiley, New York, 1996).
[53] S.M. Reimann, M. Koskinen, H. Häkkinen, P.E. Lindelof, and M. Manninen, Phys. Rev. B **56**, 12 147 (1997).
[54] J.P. Perdew and A. Zunger, Phys. Rev. B **23**, 5048 (1981).
[55] D.M. Ceperley and B.J. Alder, Phys. Rev. Lett. **45**, 566 (1980).
[56] J.P. Perdew, Phys. Rev. B **33**, 8822 (1986).
[57] R. Car and M. Parrinello, Phys. Rev. Lett. **55**, 2471 (1985).
[58] J.P. Perdew, K. Burke, and M. Ernzerhof, Phys. Rev. Lett. **77**, 3865 (1996); **78**, 1396(E) (1997).